LIGO-T980125-00-D
HYTEC-TN-LIGO-31
8/30/98

LIGO Scissors Table Static Test and Analysis Results

Eric Swensen and Franz Biehl
August 30, 1998

Abstract

Static structural tests were conducted on the LIGO scissors table to determine the force-deflection characteristics of the table assembly. Nonlinear measured force-deflection curves were observed in the test data that were confirmed by a finite element structural model. Measured nonlinear effects are primarily due to the gap spacing between hinge lugs. The distribution among individual gap spacing can have an appreciable impact on the measured static load-deflection curve. The finite element model was used to validate the test data and provide some insight into the measured nonlinear static response curves.

HYTEC Inc.
110 Eastgate Dr., Ste 100
Los Alamos, NM 87544
(505) 661-3000 / Fax (505) 662-5179

LIGO PROJECT

Table of Contents

List of Figures

1. Summary

The purpose of this report is to present test data and interpretation plus analysis results of the LIGO scissors table assembly. A special test fixture was designed to facilitate application of shear loads to determine the effective table stiffness. A finite element model was developed to calculate and validate the measured stiffness characteristics. The analytical finite element model displayed a similar nonlinear force-deflection curve as observed in the test data. The results of these investigations have a bearing on the selection of the appropriate structural material to achieved the desired LIGO assembly performance.

2. LIGO Scissors Table Description

Figure 1 is an isometric sketch of the LIGO scissors table. Figures 2 through show details of the upper plate, upper hinge, lower hinge, and lower plate.

Figure 1: Isometric view of scissors table assembly.

Figure 2: Detail view of upper plate.

Figure 3: Detailed view of upper hinge plate.

Figure 4: Detailed view of lower hinge plate.

Figure 5: Detail view of lower plate.

3. Test Model

3.1 Test setup

Figures 6 through 8 show the general test setup arrangement.

Figure 6: test setup arrangement.

Figure 7: test setup

Figure 8: test setup

3.2 Test instrumentation arrangement

Figure 9 is schematic layout of the test instrumentation layout.

Figure 9: test instrumentation layout.

3.3 Test data acquisition system

The test data acquisition system is displayed in Figure 10.

Figure 10: test data acquisition system.

3.4 Test procedure

The test procedure consists of the following steps.

4. Test Results

Test results were obtained for a stainless steel scissors assembly model and for a 1024 aluminum.

4.1 Stainless steel model

Figures 11 through 15 show force-deflection trends for the stainless steel scissors assembly.

Figure 11: Stainless steel model test results.

Figure 12: Stainless steel model test results.

Figure 13: Stainless steel model test results.

Figure 14: Stainless steel model test results.

Figure 15: Stainless steel model test results.

4.2 Aluminum model

Figures 16 through 20 present force-deflection plots for the Aluminum scissors models.

Figure 16: Aluminum model test results.

Figure 17: Aluminum model test results.

Figure 18: Aluminum model test results.

Figure 19: Aluminum model test results.

Figure 20: Aluminum model test results.

4.3 Test results discussion

4.3.1 Initial deflections under small loads

4.3.2 Observed nonlinear effects

5. Analytical Finite Element Model

A finite element model was generated to examine some effects seen in the test data such as the nonlinear force-deflection characteristics. COSMOS/M[3] finite element code was used in the simulations. The model simulates free rotating hinges and engaging gaps between adjacent hinge members as well as the structural aspects of the assembly plate members. The model exhibits the nonlinear force-deflection character measured in the test models that occurs when subsequent gaps close between adjacent load bearing hinge members. As in observed in the test model, the structure becomes less compliant (increase stiffness) as the load increases as the gaps between adjacent hinge members close and more parallel load paths are created in the model. A simple three-hinge model was generated first facilitate the development of the comprehensive model.

5.1 Three hinge model

A finite element model simulating three-hinge assembly was used to develop the element configuration that permits free hinge rotations. The model is displayed in Figure 21 followed the displaced configuration in Figure 22. Two vertical parallel springs are placed between the upper and lower plates to resist the applied vertical load. As seen in Figure 21, the model allows free hinge rotations about the hinge axes.

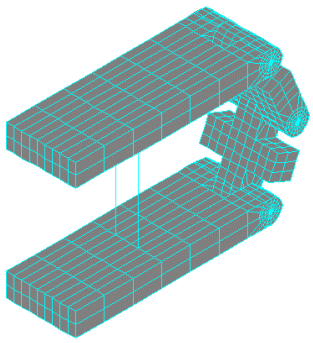

Figure 21: Finite element three hinge model.

Hinge pins are simulated using linear three dimensional beam elements (BEAM3D) while all remaining structure is simulated with linear 8 node linear isoparametric solid (SOLID) elements. Free hinge rotations is achieved by the very small (0.001 inch) beam elements between adjacent hinge members. Although the beam elements carry rotation degree-of-freedom (DOF) about their beam axis, this DOF cannot be transmitted to the surrounding solid element simply because solid elements do not have node rotation DOF. The beam rotations are restrained so that the rotation DOF avoids a singularity in the subsequent assembly stiffness matrix. The beams carry the shear and bending forces between adjacent hinge members.

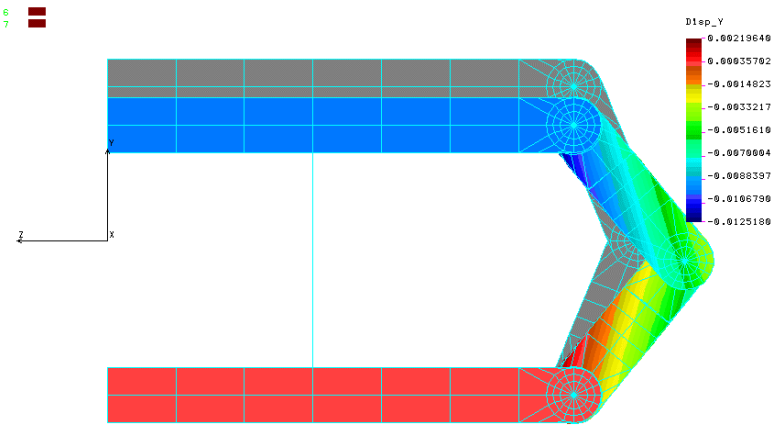

Figure 22: Three hinge model undeformed (grey elements) and superimposed deformed shape due to applied vertical load.

5.2 Comprehensive finite element model

A comprehensive finite element model was generated to simulate the scissors table assembly. One side only is simulated using symmetric boundary conditions along a plane of symmetry as shown in Figures 23 and 24. In addition to the free rotation hinge simulation from the three-hinge model, gap elements between adjacent hinge members is simulated to permit increasing number of contacting hinge members with increasing loads. It is this effect of increasing contacting hinge members that lead to the nonlinear force-deflection functions. As more hinge members are in contact, the effective longitudinal stiffness increases. The gap arrangement is achieved by allowing axial freedoms in the beam hinge elements and gap elements set to estimated gap values between the beam nodes.

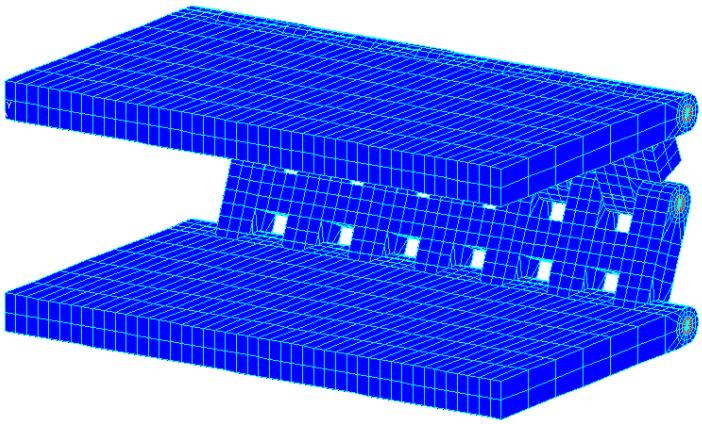

Figure 23: Scissors table finite element model showing element details.

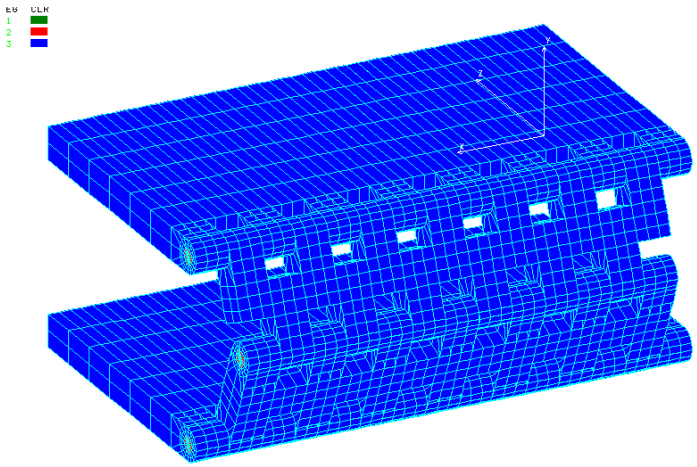

Figure 24: Alternate view of scissors table finite element model.

5.3 Gap size distribution

A series of gap sizes are assumed that are within the range of possible gap magnitudes based upon the component engineering drawings. An initial load path consisting of a closed gap along each hinge line is required from the top to bottom plate to initiate an analysis. Additional gaps close as the applied load is increased until all gaps are closed and subsequent loads generate a straight-line load-displacement curve labeled "effective table stiffness." The total number of load transfer adjacent hinge lugs in one load direction is 20; three are defined as initial load paths so that 17 remain for gap assumed gap size. Two sets of gaps were examined as shown in the following table. The same gaps were chosen for the different steps in gap distance.

Number of gaps	Small gaps (in)	Large gaps (in)
5	0.0005	0.0015
5	0.001	0.002
5	0.0015	0.003
2	0.002	0.0035

Table I: Finite element model assumed gap size distribution.

6. Finite Element Model Results

6.1 Typical displacement results

Figures 30 and 31 show a typical color contour plot of displacements at loads of 2500 and 10,000 lbf, respectively. Examination of Figure 30 reveals the original assumed load path (closed hinge gaps) as demonstrated by similar color contours. In particular, the upper row extreme right hinge and center hinges in the middle row and bottom row are fixed in the closed position. As additional hinges close in Figure 31, the colors change. It should be noted that subsequent closing of hinges will not be indicated by similar color

contours simply because gap closure displacements are contained in the motion indicated colors.

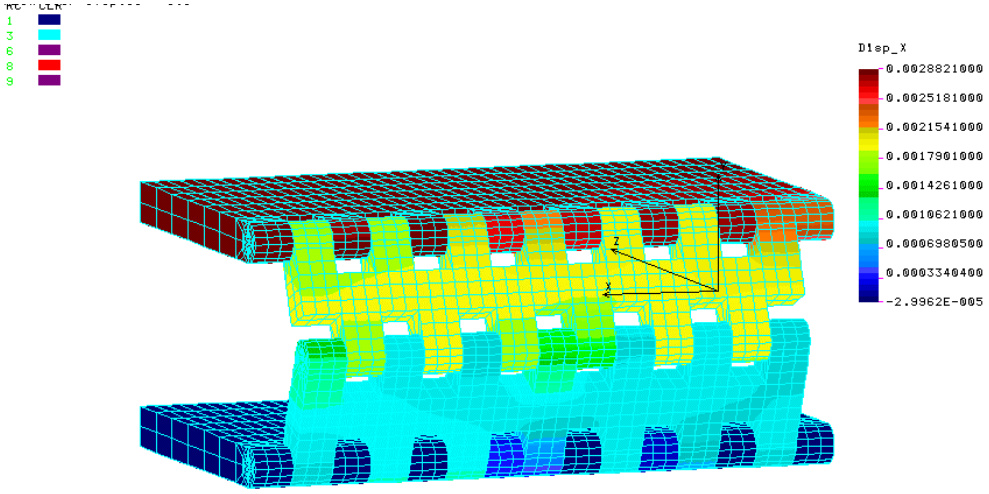

Figure 30: Displaced shape contour plot at 2500 lbf load.

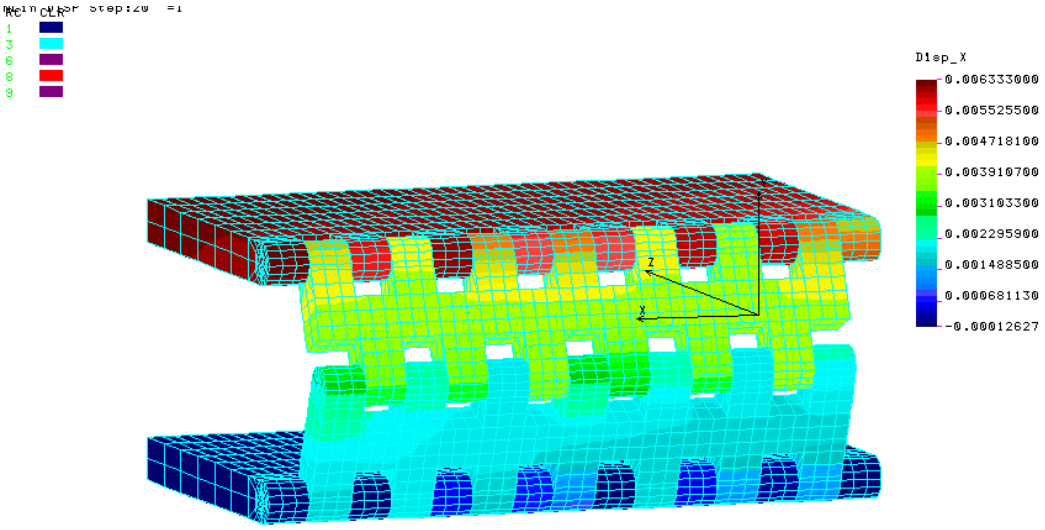

Figure 31: Displaced shape contour plot at 10,000 lbf load.

6.2 Stainless steel model

Figure 32 shows the stainless steel load-displacement curve for both the small and large gap configurations. For the large gap case, 9 gaps are closed at about 5000 lbf and 12 gaps are closed at 10,000 lbf. In the small gap case, 9 gaps are closed at about 3600 lbf while 15 of the 17 gaps are closed at 10,000 lbf. The nonlinear curves occur by increasing numbers of gaps closing as the applied load increases. Complete gap closing that lead to linear load-displacement require larger applied loads. These larger load results are presented in section 6.3.

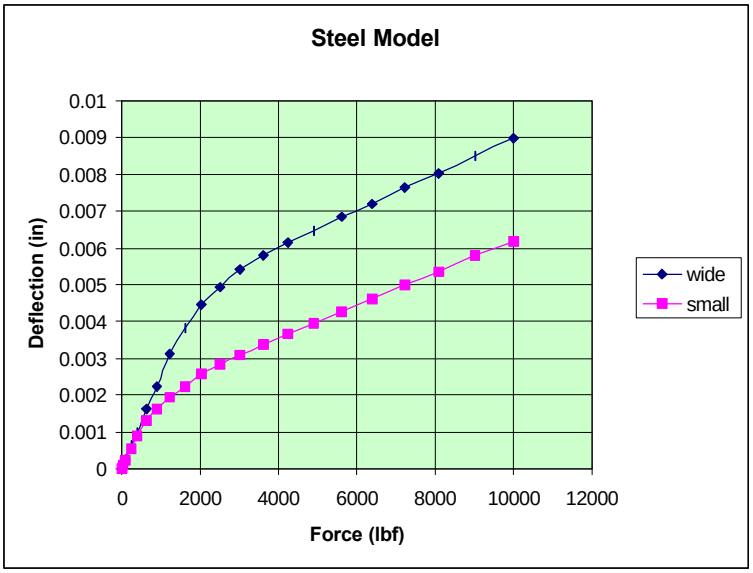

Figure 32: Stainless steel finite element model load-deflection curves for wide and small gap dimensions.

6.3 Aluminum model

Figure 33 presents the finite element model results for the aluminum model depicting the displacement as a function of applied load. For the large gap case, 9 gaps are closed at about 3600 lbf and all gaps are closed at 10,000 lbf. For the small gap model, 11 gaps are closed at 3600 lbf and all gaps are closed at about 9000 lbf.

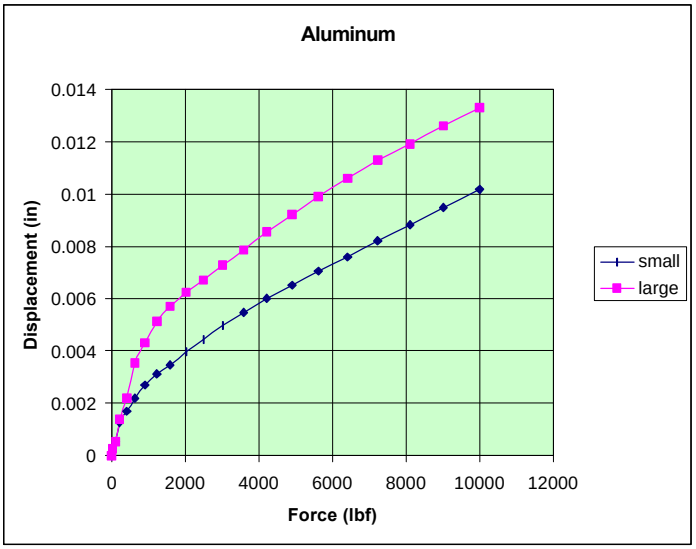

Figure 33: Load-deflection curves for the aluminum finite element model.

6.4 Stainless steel and aluminum model comparison

Load-deflection curves for stainless steel and aluminum are shown at higher loads in Figure 34. The straight line stiffness (force divided by difference in displacement) values are 2.96E6 lbf/in and 1.40E6 lbf/in for the steel and aluminum models, respectively.

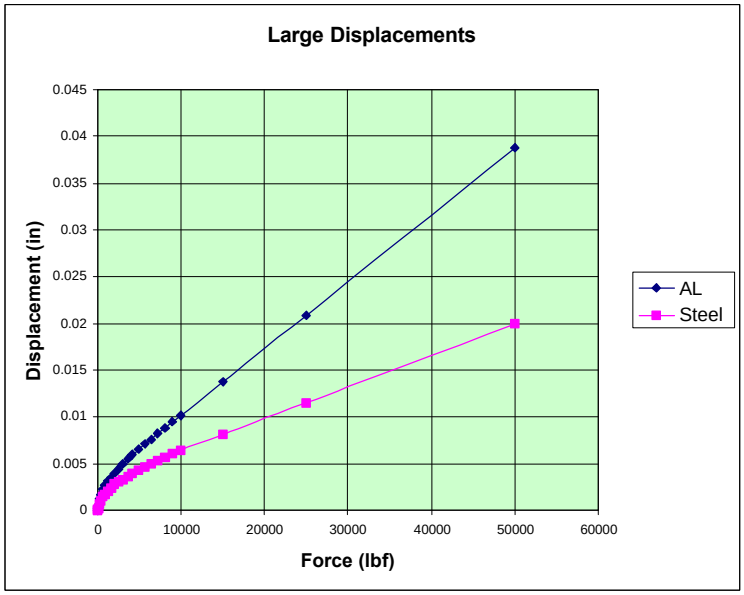

Figure 34: Force-deflection curves for stainless steel and aluminum models at higher force levels (small gaps).

As indicated previously, the hinge pins are made of a silicon brass and bronze metal having a modulus of 15E6 psi. Corresponding modulus for aluminum is 11E6 psi and for stainless steel is 30E6 psi; thus, the effective stiffness for aluminum model is increased while the effective stiffness for the steel model is decreased by the presence of the hinge pins. Replacing the brass pins by aluminum and steel in the respective models produces an effective stiffness of 1.30E6 lbf/in for the aluminum model and 3.57E6 lbf/in for the steel model. As expected, the resulting stiffness ratio (steel/aluminum=2.74) is reasonably equal to the modulus ratio (steel/aluminum=2.73) for the homogeneous material models.

6.5 Parallel path stiffness

The effect of selecting the number of load paths from the top plate to the bottom plate is exhibited in Figure 35. Although it is quite unlikely that there would be integer numbers of paths, it is useful to explore this effect. It is entirely possibly that one discrete path would be present at some low load level; however, multiple load paths would require that the distribution of gaps from top to bottom hinges be nearly identical.

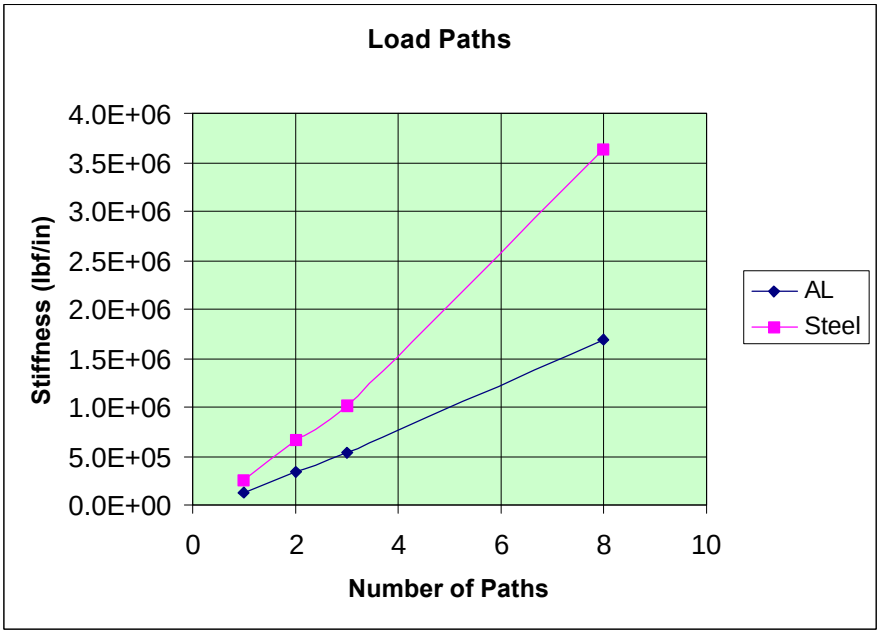

Figure 35: Effective stiffness as a function number of load paths.

7. Closed Form Models

7.1 Closed gap distribution scenario

This section examines the effect of a simple gap closing distribution on the final effective assembly stiffness (final slope of force-deflection curve). Assume that 9 of the 20 gaps on each side are closed, that the effective stiffness of each gap is the same, and that the number of closed gaps along each hinge row is variable. Effective stiffness as a function of closed gap distribution is summarized in Table II. Note that at least one gap per hinge row needs to be closed to carry the load from the top to the bottom plate. Effective stiffness in each row is a sum (parallel springs) of a single contact stiffness (Kc) and the three row total is a series connection of the three rows.

Case	Number of closed gaps			Effective stiffness
	Row 1	Row 2	Row 3	
1	3	3	3	1.0 Kc
2	3	4	2	0.923 Kc
3	5	2	2	0.833 Kc
4	4	4	1	0.667 Kc
5	3	5	1	0.652 Kc
6	6	2	1	0.600 Kc
7	7	1	1	0.467 Kc

Table II: Effective summed hinge stiffness as a function of closed gap distribution.

Tabulated results in Table II indicate that the effective stiffness can vary more than 2 to 1 for a 3,3,3 gap closure distribution to a 7,1,1 distribution. If maximum stiffness is required for best LIGO performance, then gap size distributions should be reasonably uniform from one hinge row to another.

7.2 Model effective stiffness

A finite element model of one hinge lug indicates a cantilever stiffness from 1.16E6 lbf/in at the tip, 2.60E6 lbf/in at the centerline plane, and 7.28E6 lbf/in near the root. There are 7 contact lugs along the top and bottom hinge lines and 6 along the middle hinge line. If it is assumed that all possible hinges are in contact, then the hinge line effective stiffness are the parallel (sum) of the two individual lugs in series. The respective stiffness are 1.3E6 for two contacting lugs, 7.8E6 lbf/in for the mid hinge, and 9.1E6 lbf/in for the top and bottom hinges. Three hinge rows are summed in series to give a one side stiffness of 2.88E6 lbf/in that is then doubled to represent both sides resisting the longitudinal load. As expected, the resulting stiffness (5.77E6 lbf/in) is larger than the steel assembly finite element model stiffness (3.57E6 lbf/in). This difference in stiffness is attributed to the contribution toward flexibility in the overall hinge structures.

8. Comparison of Test and Analysis Results

The simple example of gap closure distribution effects presented in the previous section illustrates the requirement that precise gap dimensions be simulated in an analytical model to achieve agreement with test results. Furthermore, the effective bending or shear deformation stiffness between two contacting hinge members depends on the effective point of contact (or multiple points of contact). In the analytical model the simulated contact point is along the pin centerline. Clearly the pin centerline would not be the contact point, however, it may be representative of an average location and thus simulate the average effective contacting hinge members bending or shear stiffness value.

The test and analytical results presented suggest that there is a very large number of potential distributions of gap size and position that influence the scissors table force-deflection curves. The analysis should be viewed as a source of explanation for some of the nonlinear effects observed in the test data.

9. Conclusions

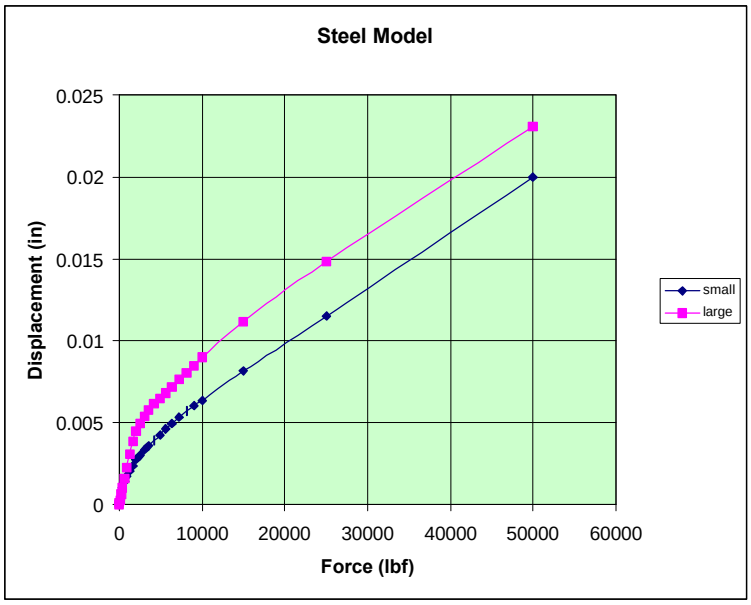

Steel model showing position of linear part is function of gap sizes

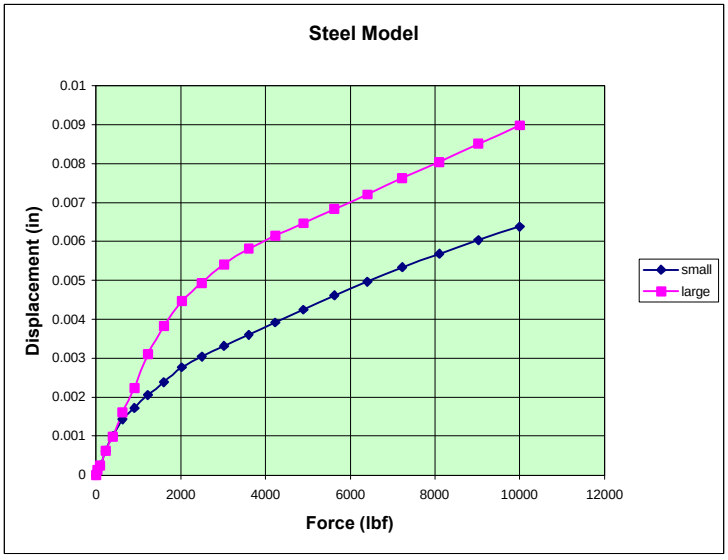

Steel model at lower loads showing nonlinear function of gap sizes

Note 1, Linda Turner, 09/03/99 02:49:07 PM
LIGO-T980125-00-D